Sensitivity of a coupled physical-biological model to turbulence: high-frequency simulations in a northern Adriatic station

Sandro Carniel[a]; Marcello Vichi[b]; Mauro Sclavo[a]

[a] Institute of Marine Sciences (CNR-ISMAR), Venice, Italy [b] Centro Euro-Mediterraneo per i Cambiamenti Climatici CMCC-INGV, Bologna, Italy

PLEASE SCROLL DOWN FOR ARTICLE

Taylor & Francis
Taylor & Francis Group

Sensitivity of a coupled physical–biological model to turbulence: high-frequency simulations in a northern Adriatic station

SANDRO CARNIEL*†, MARCELLO VICHI‡ and MAURO SCLAVO†

†Institute of Marine Sciences (CNR-ISMAR), Venice Section, San Polo 1365, I-30125 Venice, Italy
‡Centro Euro-Mediterraneo per i Cambiamenti Climatici CMCC-INGV, Via D. Creti, 12, I-40128 Bologna, Italy

This paper investigates the impacts of different turbulence models on the biological state at an ocean station in the northern Adriatic sea, named S3, comparing them with other uncertainties inherent to coupled physical–biological simulations. The numerical tool is a 1-D model resulting from the coupling of two advanced numerical models. The hydrodynamic part is modelled using the General Ocean Turbulence Model (www.gotm.net), in a version adopting state-of-the-art second-moment Turbulence Closure Models (TCMs). Marine biogeochemistry is parameterized with the Biogeochemical Flux Model (http://www.bo.ingv.it/bfm), which is a direct descendant of ERSEM (European Regional Sea Ecosystem Model). Results, obtained by forcing the model with hourly wind and solar radiation data and assimilating salinity casts, are compared against monthly observations made at the station during 2000–2001. Provided that modern second-moment TCMs are employed, the comparisons indicate that both the physical and the biological dynamics are relatively insensitive to the choice of the particular scheme adopted, suggesting that TCMs have finally 'converged' in recent years. As a further example, the choice of the nutrient boundary conditions has an impact on the system evolution that is more significant than the choice of the specific TCM, therefore representing a possible limitation of the 1-D model applied to stations located in a Region of Freshwater Influence. The 1-D model simulates the onset and intensity of the spring–summer bloom quite well, although the duration of the bloom is not as prolonged as in the data. Since local dynamics appears unable to sustain the bloom conditions well into summer, phytoplankton at the station was most likely influenced by river input or advection processes, an aspect that was not found when the S3 behaviour was adequately modelled using climatological forcings. When the focus is in predicting high-frequency dynamics, it is more likely that lateral advection cannot be neglected. While the physical state can be satisfactorily estimated at these short time scales, the accurate estimation of the biological state in coastal regions still appears as rather elusive.

Keywords: Pelagic environment; Simulation; Coastal zone; Turbulent diffusion; Physical–biogeochemical modelling; BFM

1. Introduction

It is generally accepted that phytoplankton concentration is mainly determined by the availability of nutrients, light (the photosynthetically available radiation, PAR), and

*Corresponding author. Email: sandro.carniel@ve.ismar.cnr.it

temperature, and its dynamics can be regarded as the physiological response or acclimation to these local environmental conditions [1]. However, even if these factors have been considered as the most important in controlling phytoplankton growth, their knowledge is necessary but by no means sufficient for obtaining a reasonable description of the observed phytoplankton distribution patterns. Information on light and nutrient availability can predict the potential growth of phytoplankton, but they have to be used in combination with an adequate description of the water mass dynamical evolution.

The best available description of physical processes is thus a necessary requisite for achieving significant skills in ecosystem modelling. Vertical mixing, turbulent diapycnal diffusion, and mesoscale dynamics determine the temporal variability of the upper layers and specifically how phytoplankton can use efficiently the available light and the upwelled/advected nutrients [2, 3]. This has led to the inclusion of more refined physics in coupled physical–biological models [4].

Although considerable problems exist also in correctly simulating the physical aspects of a marine site, some of the uncertainties in coupled physical–biogeochemical models are to do with the choice of the biological parameterizations, as there is little consensus on the form of the governing equations to be used. This is particularly evident in coastal ecosystems and in ROFI regions, where physical structures have shorter timescales compared with the open ocean and where the interaction with the land boundaries is relatively more important [5]. In addition, the system state is complicated by the succession of different marine species [6] and also by the development of various types of food-web interactions and microbial loop dynamics [7].

Turbulence plays a major role in shaping the vertical structure of the water column, and recent works and reviews have pointed out how the adoption of second-moment turbulence closure models (TCMs) is of central importance in purely geophysical [8] and coupled physical–biological simulations [9–13]. Nevertheless, in some of these studies, the sensitivity of different turbulence models was not explored [11–13], or high-frequency forcings were not employed [11], while in others the turbulence and/or biological models were not equally balanced in terms of complexity [9].

This paper therefore investigates some of the uncertainties related to coupled physical–biogeochemical simulations, focusing on the interaction between turbulence modelling under high-frequency forcings and the parameterization of biogeochemical processes. The effects of different modelling 'practices' (choice of TCMs and boundary conditions) are tested on a model hindcast of the physical–biological dynamics at a shallow water station in the northern Adriatic Sea during the period 2000–2001, when high-frequency physical forcings were available, as well as observational data collected approximately on a monthly base. This station has also a 'relatively abundant' biological information that can be used for assessing the coupled model skill. Important biological parameters such as macronutrient and oxygen concentrations, chlorophyll *a*, PAR, phytoplankton carbon, and primary production were measured by the CNR-Institute of Marine Sciences (CNR-ISMAR) every month [14].

2. Methods

This study was performed with a numerical model derived from the coupling of two existing models. The physics of the water column is solved by the General Ocean Turbulence Model (GOTM; for appropriate references and a list of application areas see Burchard *et al.* [15]), a state-of-the-art modelling tool that incorporates advanced closure schemes for the numerical solution of turbulence. The biology is solved with the

Biogeochemical Flux Model (BFM; http://www.bo.ingv.it/bfm), a direct descendant of the European Regional Sea Ecosystem Model (ERSEM) [16, 17] developed in the framework of the EU project Mediterranean Forecasting System Towards Environmental Predictions (MFSTEP; http://www.bo.ingv.it/mfstep). The BFM is a biomass-based ecosystem model that simulates the cycling of carbon, oxygen, and nutrients in marine systems. This approach has been applied in several regional implementations [13, 18, 19], and also to simulate the global ocean ecosystem [20, 21].

In this work, different second-moment turbulence closure models, generally considered to be a very good trade-off for geophysical applications [8, 22], were implemented with the goal to reproduce the proper state of the turbulent mixing in the water column, which affects the distribution of biota and hence its biological state.

2.1 *Physical model equations*

The major aim of GOTM is to simulate small-scale turbulence and vertical mixing in a 1-D numerical environment. The model has the possibility of being driven by observational data (surface slopes, velocities along the column, profiles of temperature or salinity, etc.) and meteorological forcings (solar radiation, cloud fraction, wind stress, etc.). The code is written in FORTRAN 90 and has a modular structure that enables it to be embedded into 3-D models, a strategy recently followed for instance in ROMS by Warner *et al.* [23]. GOTM relies on the Reynolds Averaged Navier–Stokes (RANS) hydrodynamic equations, modified for the 1-D cast:

$$
\begin{aligned}
\frac{\partial U}{\partial t} - fV &= -g\frac{\partial \eta}{\partial x} - \frac{\partial}{\partial z}\left(\overline{u'w'}\right) + v_{\mathrm{m}}\frac{\partial^2 U}{\partial z^2} \\
\frac{\partial V}{\partial t} + fU &= -g\frac{\partial \eta}{\partial y} - \frac{\partial}{\partial z}\left(\overline{v'w'}\right) + v_{\mathrm{m}}\frac{\partial^2 V}{\partial z^2} \\
\frac{\partial \Theta}{\partial t} &= \frac{1}{\rho_0 c_{\mathrm{p}}}\frac{\partial I}{\partial z} - \frac{\partial}{\partial z}\left(\overline{w'\theta'}\right) + \lambda_{\mathrm{T}}\frac{\partial^2 \Theta}{\partial z^2} - \frac{1}{\tau_{\mathrm{T}}}\left(\Theta - \Theta_{\mathrm{d}}\right) \\
\frac{\partial S}{\partial t} &= -\frac{\partial}{\partial z}\left(\overline{w's'}\right) + \lambda_{\mathrm{S}}\frac{\partial^2 S}{\partial z^2} - \frac{1}{\tau_{\mathrm{S}}}(S - S_{\mathrm{d}}),
\end{aligned}
\tag{1}
$$

where x, y, and z are the axis coordinates, $U = \overline{u}$ and $V = \overline{v}$ the averaged horizontal velocity components, t the time, f the Coriolis frequency, g the gravitational acceleration, η the sea surface elevation, $\overline{u'w'}$ and $\overline{v'w'}$ the vertical turbulent fluxes of momentum and v_{m} indicates the molecular diffusivity of momentum (very small compared with turbulent fluxes). The equations for the temperature $\Theta = \overline{\Theta}(S = \overline{S})$ denote the averaged temperature (salinity), ρ_0 a reference density, c_{p} the specific heat of sea water at constant pressure, I the solar radiation, $\overline{w'\theta'}$ $\left(\overline{w's'}\right)$ and $\lambda_{\mathrm{T}}(\lambda_{\mathrm{S}})$ the vertical turbulent flux and molecular diffusion coefficients of temperature (salinity). $\Theta_{\mathrm{d}}(S_{\mathrm{d}})$ are observed values, while $\tau_{\mathrm{T}}(\tau_{\mathrm{S}})$ are depth-dependent timescales of the relaxation source terms.

The turbulent fluxes parameterize turbulence in terms of the mean-flow quantities, e.g. $\overline{u'w'} = -K_{\mathrm{M}}(\partial U/\partial z)$. The eddy viscosity takes the form $K_{\mathrm{M}} \propto S_{\mathrm{F}}k^{1/2}\ell$, the product of a stability function (dimensionless, different for momentum or tracers, and depending on shear/stratification), a characteristic velocity (related to k, the turbulent kinetic energy TKE) and a length scale related to the size of the dominant eddies. By means of the well-known cascading relation, the length scale ℓ may be related to the dissipation rate: $\varepsilon \propto (k^{3/2}\ell)$.

Therefore, in order to obtain an estimate of the turbulent fluxes for momentum and tracers, values for the two physical quantities k and ℓ (or ε) must be found. There is a general consensus

on how to write a transport equation for k [24–26], which can be directly derived from the equations for the Reynolds stresses [26–29], neglecting advective terms and assuming down-the-gradient model for diffusion:

$$\frac{Dk}{Dt} - \frac{\partial}{\partial z}\left(\frac{K_M}{\sigma_k}\frac{\partial k}{\partial z}\right) = P + B - \varepsilon, \tag{2}$$

where $P = (-\overline{u'w'}(\partial U/\partial z) - \overline{v'w'}(\partial V/\partial z)) = K_M M^2$, is the rate of production due to the shear, with $M^2 = (\partial U/\partial z)^2 + (\partial V/\partial z)^2$, and $B = (\beta g\overline{w'\theta'} + \beta_S g\overline{w's'})$ the rate of production/destruction by buoyancy (g is gravity acceleration, β and β_S the thermal expansion coefficient), K_M is the turbulent (eddy) diffusivity, σ_k the constant turbulent Schmidt number for k. Of course, the solution of this equation requires the knowledge of ε, the dissipation rate, which we saw is a function of k and ℓ. On the other hand, the computation of the latter was in considerably less agreement. Historically, this has been done first using simple integral expressions and then moving to more complex differential equations. As will be explained in the following, the TCM takes the name from the adopted mixing length.

2.1.1 One-equation, second-moment turbulence closure models. As we mentioned briefly above, the equation for the second unknown (i.e. the dissipation length scale) remaining after the closure of the second moments in the RANS can be prescribed in different ways. For the sake of consistency, as a first guess we follow Chen and Annan [9], who employed the Xing and Davies [30] formulation $\ell = (\ell_1^{-1} + \ell_2^{-1})^{-1}$, where $\ell_1 = \kappa(\sigma H + z_0)e^{a\sigma}$ and $\ell_2 = \kappa(H - \sigma H + z_S)$, where κ is the Von Karman constant, H the total water depth, σ a normalized vertical coordinate, α an empirical constant, and z_0 (z_S) the bottom (surface) roughness lengths, respectively. This formulation allows for a larger reduction in the mixing length in the lower parts of the water column but has the main disadvantage that the length scale needs to be prescribed a priori, which is difficult in complex flow situations. A prognostic equation for the length scale would therefore be much more preferable.

2.1.2 Two-equation, second-moment turbulence closure models. These TCMs solve equation (2) for the TKE *and* an additional differential equation for a quantity involving the turbulent length scale ℓ, in which the transport equation is usually patterned after the TKE one, and from which the TCM itself borrows the name. They have become rather popular in geophysical applications in the last decades, bringing to the well-known $k - k\ell$ [26], the $k - \varepsilon$ [24] or the $k - \omega$ [25, 31, 32] examples. In this work, we will be adopting the TCM proposed in section 2.1.1 and the following three ones presented in 2.1.3, 2.1.4 and 2.1.5.

2.1.3 $k - \varepsilon$ model. The ε length scale equation is probably the most widely used today, and it is often claimed to be more applicable than others as it pertains to a physically meaningful and rather fundamental property of turbulence, the dissipation rate ε. An exact equation for this quantity can be obtained by differentiating the Navier–Stokes equation for the turbulent velocity component, as shown by Hanjalic and Launder [33] and Wilcox [34]. Without going into details (but see Lacroix and Nival [12]), the transport equation for ε has the form:

$$\frac{D\varepsilon}{Dt} - \frac{\partial}{\partial z}\left[\frac{K_M}{\sigma_\varepsilon}\frac{\partial \varepsilon}{\partial z}\right] = \frac{\varepsilon}{k}(C_{\varepsilon 1}P + C_{\varepsilon 3}B - C_{\varepsilon 2}\varepsilon), \tag{3}$$

where P, B, and ε are, respectively, the shear production, buoyancy production, and dissipation of ε, and σ_ε is the Schmidt number for the eddy diffusivity of dissipation. A set of possible

values for the empirical constants is given by Rodi [24] and Kantha [25]: $C_{\varepsilon 1} = 1.44$, $C_{\varepsilon 2} = 1.92$, $C_{\varepsilon 3} = 0.2$, $\sigma_\varepsilon = 1.159$.

2.1.4 $k - \omega$ **model.** This model, originally proposed by Wilcox [31, 34], has been noticed lately by geophysical turbulence modellers and is based on an equation for the turbulence frequency, $\omega \propto (k^{1/2}/\ell)$, a physically meaningful quantity involving the length scale. The advantage of the $k - \omega$ model is that it can be integrated through the viscous sublayer to the solid wall, without the need for wall functions, rendering it quite popular in industrial applications. The transport equation for ω can be written as:

$$\frac{D\omega}{Dt} - \frac{\partial}{\partial z}\left[\frac{K_M}{\sigma_\omega}\frac{\partial \omega}{\partial z}\right] = \frac{\omega}{k}(C_{\omega 1}P + C_{\omega 3}B - C_{\omega 2}\varepsilon). \tag{4}$$

Wilcox [31] uses $C_{\omega 1} = 5/9$, $C_{\omega 2} = 5/6$, $\sigma_\omega = 2$. The extension of this model to stratified fluids and the computations of the related empirical parameters, including $C_{\omega 3}$, have been discussed by Umlauf *et al.* [32].

2.1.5 Generic Length Scale model $k^m \ell^n$. More generally, as formalized by Umlauf and Burchard [35], it is possible to write a transport equation for a *general* quantity $\psi = (c_\mu^0)^p k^m \ell^n$ called the Generic Length Scale (GLS), and employ this as a second equation besides the consolidated equation for the TKE:

$$\frac{D\psi}{Dt} - \frac{\partial}{\partial z}\left(\frac{K_M}{\sigma_\psi}\frac{\partial \psi}{\partial z}\right) = \frac{\psi}{k}(c_{\psi 1}P + c_{\psi 3}B - c_{\psi 2}\varepsilon). \tag{5}$$

The quantities σ_ψ, $c_{\psi 1}$, $c_{\psi 2}$, and $c_{\psi 3}$ are closure constants, and K_M is the eddy viscosity. As a consequence, all the above written length-scale equations become subsets of the GLS notation. Using $p = 3$, $m = 3/2$, $n = -1$, we obtain $\psi = (c_\mu^0)^3 k^{3/2} \ell^{-1}$, recovering the $k - \varepsilon$ model. Using $p = -1, m = 1/2, n = -1$, we obtain $\psi = (c_\mu^0)^{-1} k^{1/2} \ell^{-1}$, recovering the $k - \omega$ model.

Kantha [25] reviewed the length-scale equation formulations demonstrating that well-known difficulties in some of the traditional approaches are due to the way in which the diffusion term is modelled, while Kantha and Carniel [36] demonstrated how the GLS default version proposed in GOTM ($m = 1$ and $n = -0.67$) leads to $\psi = k\ell^{-2/3} = (k^{3/2}\ell^{-1})^{2/3}$ and therefore working for a quantity ε^q where $q = 2/3$. Despite the interesting debate on the proper formulation of a GLS (for excellent reviews, see Umlauf and Burchard [8] and integrations from Kantha [22]), in this study we retain the original setup proposed by Xing and Davies [30] and called by the authors '*gen*', both because it is the best guess suggested by Umlauf and Burchard [35] and with the purpose of helping comparisons with other studies [23] as well.

The TCMs adopted in this work include an additional mixing effect due to breaking of surface gravity waves in the upper ocean, which injects turbulence directly into the upper few meters of the water column. Following recent modelling approaches [15, 37–40], the surface wave breaking effect has been included by prescribing an additional energy injection in the upper boundary condition $-K_M(\partial k/\partial z) = -\eta u_*^3$, where $\eta \approx 100$ is an empirical parameter [41], and u_* is the surface friction velocity.

2.2 *Biogeochemical model*

The BFM follows the chemical functional family approach described thoroughly in Vichi *et al.* [20]. Each living functional group represents an implicit size class of organisms, all

sharing similar physiological/ecological processes such as growth, ingestion, respiration, excretion, and grazing. The exchanges among living functional groups and the other non-living organic and inorganic components are modelled in terms of carbon and macronutrient flows. Each state variable is defined as a multi-dimensional vector that contains the concentrations of C, N, P, and (when required) Si and chlorophyll. The principal functional groups in the pelagic environment are unicellular planktonic autotrophs, micro- and mesozooplankton and heterotrophic aerobic/anaerobic bacteria. The model also simulates the dynamics of nitrate (NO_3), ammonium (NH_4), orthophosphate (PO_4), biogenic silicate (SiO_2), oxygen (O_2), carbon dioxide (CO_2), and dissolved/particulate non-living organic matter (DOM, POM). Since this work mainly focused on the pelagic dynamics, the benthic part of the BFM was not used in the simulations.

In BFM, there are up to four functional sub-classes of phytoplankton: diatoms, autotrophic nanoflagellates, picophytoplankton, and partially inedible large phytoplankton. The groups have been identified as representative of the wide spectrum of functionalities and sizes of planktonic algae in the Adriatic [14].

The dynamical equation for the biogeochemical state variables is similar to that for the physical tracers

$$\frac{\partial C}{\partial t} = -\frac{\partial}{\partial z}(\overline{w'C'}) + \lambda_C \frac{\partial^2 C}{\partial z^2} + \left.\frac{\partial C}{\partial t}\right|_{\text{bio}} \tag{6}$$

where C is the concentration of any chemical family (e.g. dissolved inorganic nutrient or carbon content in phytoplankton). The biogeochemical source term, the last on the right-hand side, is different for each state variable and is thoroughly described in Vichi *et al.* [20].

The BFM model is freely available to the scientific community, and the full documentation and FORTRAN codes can be downloaded from the model website http://www.bo.ingv.it/bfm.

3. Model setup and data availability

The observation station S3 in the north-west Adriatic Sea (45.25° N, 12.77° E, figure 1) is located approximately 37 km offshore in waters 28 m deep. The station is close to the middle of the northern Adriatic cyclonic gyre [42] and was chosen for this study because of the availability of extensive hydrological and relatively abundant biochemical measurements made there during recent years. The S3 area has always been considered as representative of the whole sub-basin [43], reflecting conditions typically considered to be those of an open sea area, being sufficiently far away from the influence of the Po river discharge (approx. 1500 m³ s⁻¹ per year on average) and therefore less influenced by riverine discharge. Nevertheless, the prevailing winds are particularly important in determining the often sudden changes in the vertical structure of this shallow water system [44, 45].

From the biological point of view, the S3 station has been studied in several observational campaigns in the past few years: PRISMA I, INTERREG I, INTERREG II initiative, ADRIA02-03. This work was done using a subset of the data recently made available by Bernardi-Aubry *et al.* [14] and Pugnetti *et al.* [46]. The data cover the period 1999–2001 with roughly a set of observations for each month. In their study, the S3 is again classified as an oligo-mesotrophic station, only sporadically influenced by the river Po outflow, with a rather low level of primary productivity. The highest phytoplankton abundance was observed in the first half of the year (March–April), mainly due to diatoms and nanoflagellates, species generally observed in the western Adriatic. While no meteorological data were collected at the station itself, a complete set is available from an automatic weather registering (AWR) station of CNR-ISMAR in Venice, about 25 km NW from the study site.
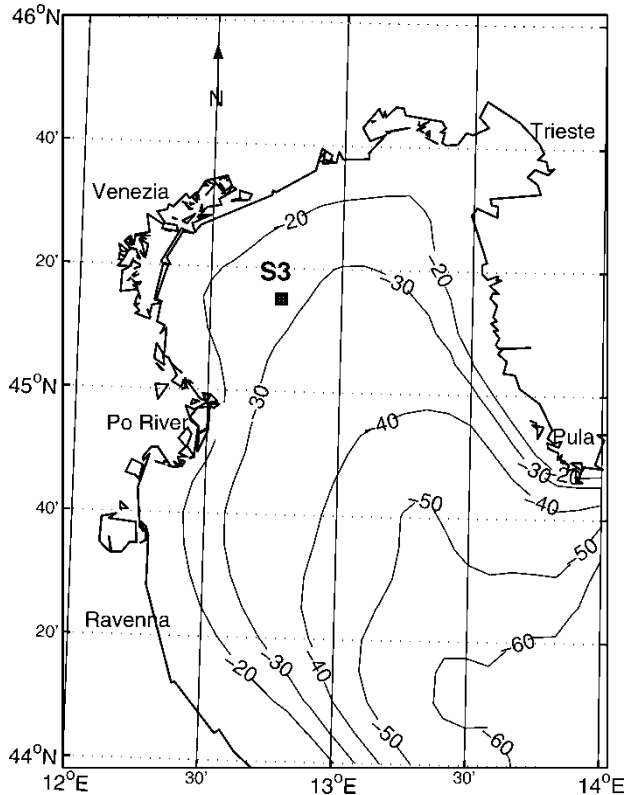
Figure 1.   Location of the Station S3 in the northern Adriatic Sea. Depths are in metres.

We preferred this data set to that available at the 'Acqua Alta' CNR platform, since the latter, although relatively closer in terms of distance, suffered from measurements gaps in the period selected for the simulations. The hourly averaged quantities were used to derive the meteorological forcing needed by the physical model to simulate the seasonal evolution of the water column from 17 January 2000 to 14 December 2001, although the results are discussed only for the year 2001 time-slice. Since wind velocities registered at the AWR station generally underestimate the prevailing winds over the sea, the wind speed and directions were obtained from a recording instrument in the proximity of Chioggia inlet (25 km SW of S3 station) operated by the Venice municipality. Hourly wind data were transformed into wind stresses for input into GOTM using a stability-dependent drag coefficient. The daily averaged value of cloud coverage, necessary to compute the net radiative heat fluxes, was obtained following the Reed formula [47] using day-of-the-year, latitude and measured solar insolation.

   The water column is discretized into 29 vertical levels, with a higher resolution in the proximity of the surface. The time step for the numerical integration is 100 s. In all the model simulations, there is *no* assimilation of temperature, and so the last parameterization term in the corresponding equation in equation (1) is set to zero. Heat fluxes are dynamically computed by the model using the incoming solar radiation and the cloud coverage values. On the other hand, since no reliable precipitation data were available, instead of computing the seasonal evolution of salinity in the mixed layer, measured values were assimilated by means of a relaxation technique as shown with a relaxation time of 1d.

3.1   *Initial and boundary conditions*

The initial temperature and salinity profiles were obtained from the January 2000 CTD cast, which shows a completely mixed water column at a temperature of about $10\,°C$. Generally, climatological 1-D models are only slightly sensitive to the initial conditions of the pelagic biological components, and the time evolution of the state variables reaches a steady state within a few years of integration [19, 48–50]. Not much information is available in the literature about the model behaviour in the case of realistic high-frequency forcing functions, although there are indications that adjustments of the pelagic components are fast [51]. With the aim of integrating the coupled model for year 2001, the physical simulations were performed in the period 2000–2001 starting on January 2000 and using various combinations of initial conditions for the biological state variables, assumed to be homogeneous in the vertical. All the simulations nearly converged to the same values at the end of the first year of integration. These final values were used to restart the model for the year 2001 except for the phytoplankton biomass. The initial carbon biomass of each phytoplankton group was derived by multiplying the observed total phytoplankton carbon [46] by the relative abundance obtained at the end of the spin-up run. Specifically, data reported a homogeneous value of $10\,\mathrm{mg\,Cm^{-3}}$ for total plankton carbon, and the applied proportion was 60% diatoms, 20% flagellates, and 20% picophytoplankton.

As for physical components, the biological equations need the specification of adequate boundary conditions (BCs), which in the particular case of macronutrients also incorporate the effects of land-derived sources into the models. Two choices are generally available: the Dirichlet BC (DBC), which clamps the value at the boundary to a fixed one, and the Von Neumann BC (NBC), which specifies the flux at the boundary. Some authors, in the case of open ocean areas where nutrients are imported in the euphotic zone due to changes in mixed layer depth, prescribe a zero boundary flux at the surface [10]. However, in other modelling cases, while the physical BCs are generally discussed extensively, the possible use of BCs for nutrients is not clearly indicated [9, 11]. We investigated the effect of both DBC and NBC; in the former $C = C_{obs}$; in the latter, the matter flux is computed through a nudging function $F_C = (\delta/\tau)(C_{obs} - C)$, where δ is the depth of the first discretized model layer, and τ a relaxation timescale. In both cases, as common practice in the absence of other information, we linearly interpolated the measurements to reconstruct a value for the observation when not available at the desired time step. Since the model does not consider the benthic part, bottom BCs were set to zero-flux for all components except for the variables that sink in the water column (diatoms and particulate detritus).

4.   Results

The set of parameters used in previous Adriatic Sea models [19, 52] was applied to the coupled ecosystem model. The results shown here focus mainly on the phytoplankton dynamics, since there is a lack of information on the zooplankton seasonal evolution at the station. From the large number of simulations performed, we present a set of experiments shown in table 1.

In the sensitivity studies described below, previous data [14, 46] have been used as a benchmark for comparing the simulation results. In order to give an objective measure of the departure from observations and of the skill of each simulation experiment, we computed root mean square errors and incremental errors for different runs. The non-normalized root

Table 1. Summary of the sensitivity experiments.

Run	TCM	Nutrient BC	Other forcings
T1	$k - \varepsilon$	NBC ($\tau = 1$ d)	Every 1 h
T2	$1 - $ eq	As above	As above
T3	gen	As above	As above
T4	$k - \omega$	As above	As above
T5	$k - \varepsilon$	As above	Averaged wind data (6 h)
F1	As above	NBC ($\tau = 0.1$ d)	Every 1 h
F2	As above	DBC	As above
F3	As above	NBC ($\tau = 1$ d)	Wind as above
			Inclusion of ISM data

mean square error is defined as:

$$\text{rmse}_i = \sqrt{\frac{1}{n} \sum_{k=1,n} (\Omega_{i,k}^{\text{M}} - \Omega_{i,k}^{\text{O}})^2}, \qquad (7)$$

where i is the discrete time index of the observations, n the number of (observed) vertical levels, and $\Omega_{i,k}^{\text{M}}$, $\Omega_{i,k}^{\text{O}}$ the model and data values at the i, k indices, respectively. The incremental error time series is computed for the generic run X with respect to a reference simulation R as:

$$\gamma_i^X = 100 \cdot \frac{\text{rmse}_i^X}{\text{rmse}_i^R} - 100, \qquad (8)$$

where rmse_i^X and rmse_i^R are the error time series from equation (7) for the given simulation X and for the reference run R, respectively. The incremental error is zero if the two rmse are the same, less than zero if the simulation performs better than the reference, and greater than zero if the simulation performs worse than the reference. If the simulation X matches the observation perfectly, then $\gamma_i^X = -100$ %.

4.1 *Sensitivity to TCMs*

The first set of sensitivity studies focuses on the turbulent transport term of equation (6) by changing the TCM formulation. Runs T1–T4 (table 1) were performed, adopting the TCMs above described in section 2.1, adopting the NBC for the biological model. Run T5, dealing with the reduction in the frequency of the wind forcing, was also added.

Several authors have shown a significant sensitivity of the biological components to the frequency of forcing functions [9, 12, 53]. We do not present the results of averaging the forcing functions over very large periods, which can be expected to change the physical structure significantly: instead, we present results after having averaged the hourly data over an interval of 6 h, a frequency generally available from numerical weather prediction models. This experiment is presented together with the other TCMs because it essentially affects the shear production of turbulence modifying short-term mixing events.

Since it is generally assumed that in numerical marine ecosystem, model changes in the physics are reflected in the biological activity, it is particularly interesting exploring the effects of the different TCMs on the temperature structure of the water column. The temperature evolution is compared with the available data at two reference depths (0.5 m and 15.5 m) in figure 2. In general, the modelled sea surface temperatures (SSTs) are in very good agreement with the observations, despite a slight overestimation during the autumn period. T1 and T3
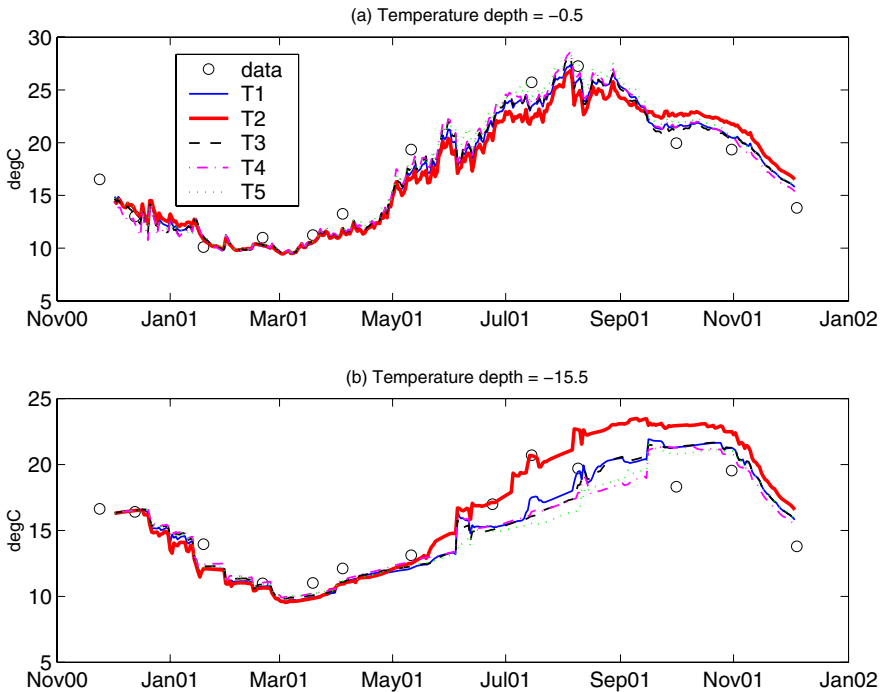
Figure 2. Observed and simulated temperature at (a) the surface and (b) -15.5 m depth. The legend is explained in table 1.

are almost indistinguishable from each other, in concert with the conclusions in Kantha and Carniel [36]. Also, T4 and T5 perform equally well, suggesting that six-hourly wind forcing is good enough for simulating the observed monthly variability. Experiment T2 shows that the performance of the one-equation TCM is poor compared with two-equation TCMs; this behaviour is more evident in the bottom layers, where we find a major sensitivity to this choice. Despite the differences in their formulation, it is evident that all TCMs are capable of reproducing the sensitivity studies' 'T' with a good degree of accuracy. One conclusion is that, when adopting realistic high-frequency forcings, the choice of the TCMs seems to have a minor impact on the evolution of the physical properties.

Indeed, this is also reflected in the biological components. Figure 3 depicts the comparison between the hindcasts of the total phytoplankton carbon (sum of the carbon components of diatoms, flagellates and picoplankton) and the observations at the surface and in the region of the pycnocline. The coupled model seems to be only partially able to match the observations irrespective of the TCM used, although care must be taken in the time extrapolation of the details of the seasonal variability from monthly frequency measurements. While the timing of the surface spring bloom (figure 3, upper panel) is reasonably well predicted, it is not sustained sufficiently during the spring. This occurs with all the TCMs, which indicates that this biomass production is independent of the turbulence model used. Instead, apart from a slightly higher April peak, the onset and decay of the bloom at 15.5 m are very well simulated by all the TCMs, with T4 and T5 showing some deviation with respect to the others.

The low sensitivity of the temperature hindcast to the choice of the TCMs is confirmed by the analysis of the incremental error (see equation (8)) shown in figure 4a. Since the results in figure 2 are so close to each other, we chose as a reference run that which adopts the $k - \varepsilon$
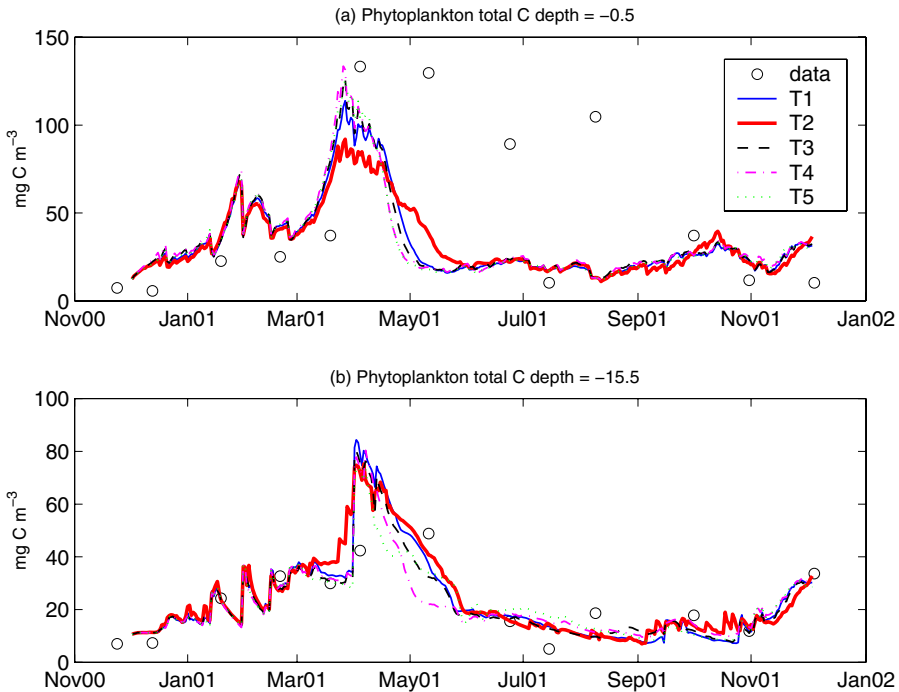
Figure 3.   Observed and simulated total phytoplankton carbon at (a) the surface and (b) −15.5 m depth. The legend is explained in table 1.

(run T1), in accordance with authors who support that this TCM can be derived rigorously from the Navier–Stokes equation.

Compared with the results of T1, runs T3, T4, and T5 show some improvement during the period January–June, but conversely they also show a somewhat poorer performance during the summer. However, it is evident that the incremental error is clustered around zero, confirming that the behaviour of the different TCMs selected is very similar. Run T2, based on a one-equation model, is the only exception and presents significant incremental errors with respect to T1. This trend is evident mainly in the post-spring period, when the water column starts to stratify, and the error reaches a maximum at 240%; and at the end of the summer, when the thermocline erosion begins, and the excessive mixing of the one-equation model results in larger mean temperatures. The incremental error of phytoplankton carbon shown in figure 4b reinforces the conclusions drawn from figure 3. The incremental error oscillates between −20 and +20%, suggesting that the different TCMs do not significantly affect the biomass distribution in the investigated period.

Therefore, the choice of the TCMs among the proposed set of state-of-the-art TCMs to compute the turbulent transport term in equation (6) does not seem to have any major impact on temperature evolution or on the biogeochemical variables. Comparisons have been performed for all the model variables, and the ranges of sensitivity to the TCMs were always within 20%. In particular, none of the TCMs could improve the description of the observed system behaviour during the period. The largest deviations from data are observed at the surface where, in contrast, the physics is correctly simulated. Since the 1-D model configuration adopted is not able to simulate lateral advection processes, a likely hypothesis is that they are related to the external surface forcings of biological relevance such as the specification of
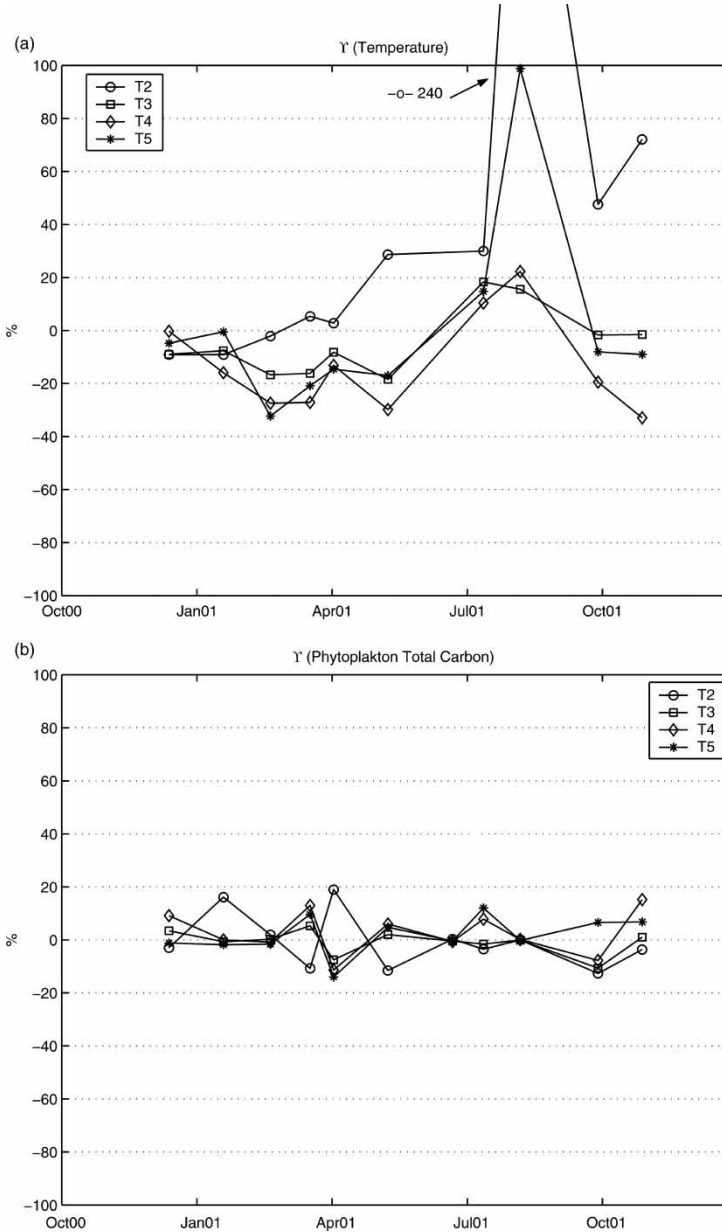
Figure 4.   Incremental error for (a) temperature and (b) phytoplankton total carbon.

alloctonous nutrient inputs, probably riverine inputs. We will return to this in more detail in the next section and in section 5.

4.2   *Sensitivity to external inputs*

The second set of experiments concerns the application of different BCs and other significant external forcings that may affect the results of the realistic simulation of a ROFI. Figure 5 shows
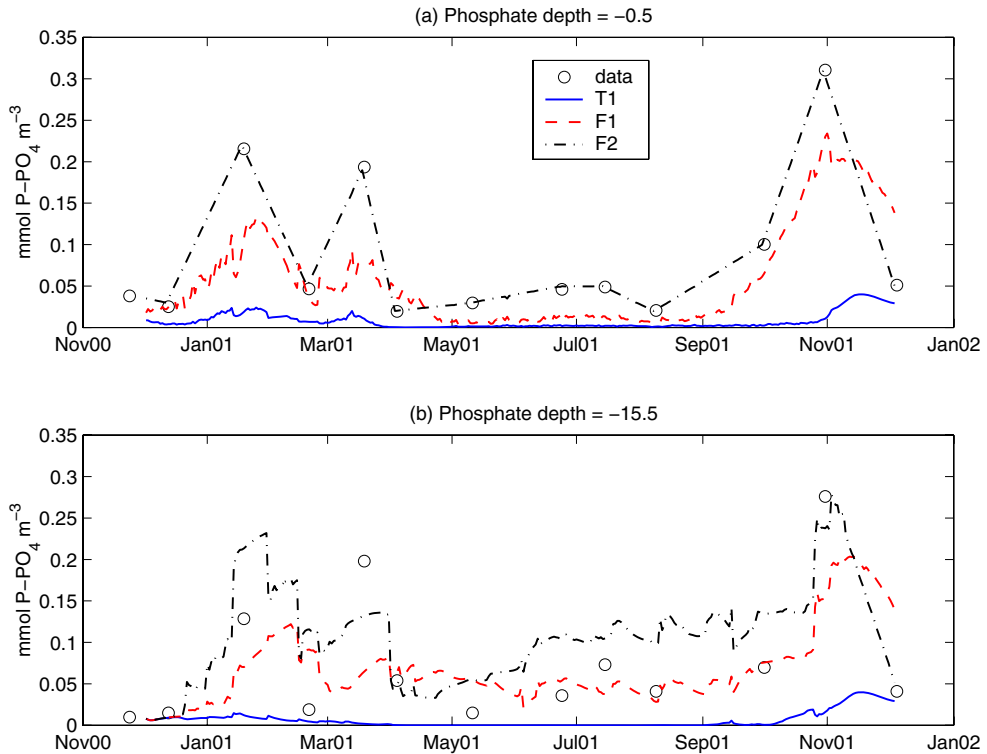
Figure 5.   Observed and simulated phosphate concentrations for the sensitivity studies on the choice of BCs: (a) surface (b) -5.5 m depth. The legend is explained in table 1.

the time series of observations of surface phosphate compared with the model results for Runs T1, F1, and F2. Runs T1 and F1 both use NBC with a virtual nutrient flux derived from the nudging equation presented in section 3.1 using the relaxation timescales given in table 1. Simulation F2 is a straightforward application of DBC, so the resulting nutrient surface evolution shown in figure 5a is not surprising. On the other hand, when applying an NBC, a decrease in the relaxation time constant of the equation for F_C (as was done from Run T1 to Run F1) leads to a substantial increase in the modelled concentration. The concentration in the middle layer (figure 5b) is best simulated with Run F1, while F2 overestimates both the winter and summer values. T1 is instead always below the observations.

An interesting result is the response of the phytoplankton, depicted in figure 6a as total carbon. Pugnetti *et al.* [46] reported a linear dependence of the biological model to variations in the nutrient loads. In our case, we see that the changes in BCs leads to a significant nonlinear response of the phytoplankton. With the use of DBC (Run F2), phytoplankton dynamics are strongly constrained by the nutrient data, which in our dataset present a maximum at the beginning of 2001, probably due to flooding in late 2000. Therefore, the two winter peaks in Run F2 are a direct consequence of high nutrients (especially silicate, not shown), sustained by the capacity of diatoms to efficiently utilize the low light levels. Run F1 shows an intermediate behaviour, but the shorter timescale of the nudging flux allows the phytoplankton to reach the large peak in middle March. This bloom is thus induced by the use of the data, although in this case we applied a very simplistic nudging but often used method, and more sophisticated assimilation schemes might be able to merge more properly with the ecosystem
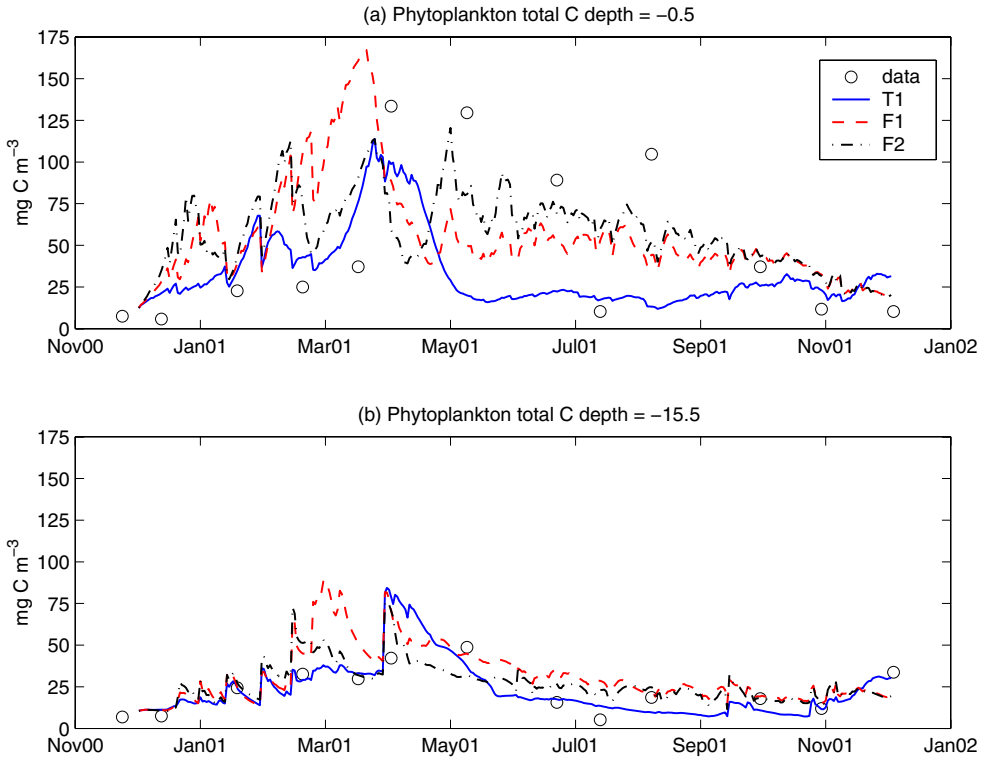
Figure 6. Sensitivity of the total phytoplankton carbon to the nutrient BCs at the surface (a) and at −15.5 m depth (b). The legend is explained in table 1.

model dynamics. Finally, it is interesting to note that, apart from the March peak in Run F1, the middle layer (figure 6b) is not particularly sensitive to the changes in surface BCs.

Rivers may not only affect the input of new nutrients into the system but also influence the light climate by changing the extinction coefficient through high concentrations of inorganic suspended matter (ISM). Vichi *et al.* [19] found a significant sensitivity of the biochemical variables in their climatological experiments after the introduction of climatological profiles of ISM; generally, the match with seasonal observations improved, especially in the winter period, although a significant site-dependent response was also observed.

Since, for this period of the simulation, it is likely that the river may be influencing the local optical conditions, we performed some additional experiments to assess the relevance of this factor in a realistic simulation. Figure 7 shows the carbon content in flagellates from Run F3, which is equivalent to Run T1 but with the addition of ISM data in the computation of light extinction coefficients. The mean water-column concentration of ISM, shown in the inset of figure 7, is essentially following the evolution of surface nutrients in figure 5, with a relative maximum during late winter/early spring, and an absolute maximum during autumn 2001. The ISM data lead to a delay of the spring phytoplankton bloom by a few weeks (dashed line). This occurs especially in flagellates, because this group is particularly sensitive to light and finds less favourable conditions which delay the onset of, and modify the shape of, the bloom. We can expect that the phytoplankton behaviour would be even more affected if high-frequency data were used, instead of linearly interpolated monthly data as was done in this experiment.
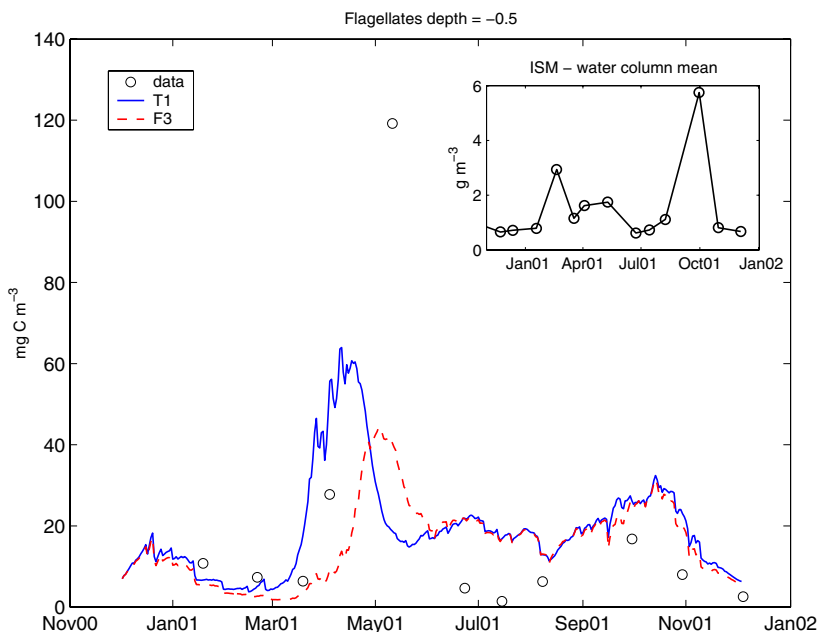
Figure 7.   Sensitivity of the surface biomass of flagellate to the inclusion of ISM (Run F3). The legend is explained in table 1.

5.   Discussion

This work mainly investigated the way in which a coupled 1-D physical–biological model can be affected by vertical dynamics of turbulence and by the imposition of external boundary conditions.

Results presented in Section 4.1 indicated how the mixed layer evolution and the thermal cycle of the S3 station can be fairly well reproduced by 1-D models, provided the availability of state-of-the-art TCMs. The analysis of the modelled temperature and diffusivity fields obtained highlighted that, if in many idealized cases the use of a particular length scale heavily influences the vertical mixing [28], in a realistic simulation where several different components are called into force (wind, solar radiation, salinity, etc.), recent TCMs have converged to an acceptable degree. Moreover, the adoption of a one-equation TCM, albeit less computationally expensive, should be considered as no longer acceptable within these categories of investigating tools, and therefore progressively set aside. Still, progress should be made to improve the modelling of the surface layer dynamics and of the thermocline region. Namely, inclusion of Langmuir effects or a better parameterization of surface wave breaking could improve surface-modelled values [54].

Despite some particular situations where all TCMs fail to accurately reproduce the temperature structure, the overall rmse values are remarkably low. The effect of the adoption of TCMs on the biochemical results is generally not very informative, a conclusion however that should by no means be considered trivial. Indeed, other authors claimed in previous studies [9] that deviations in physical small-scale processes had indeed direct and large effects on the biochemical counterpart, possibly reaching these findings since they were using both simplified TCMs and biological models. As an example, the total phytoplankton incremental error in Run T2 was shown not to be correlated with corresponding large errors in the modelled temperature (increment of 240%), which are a direct consequence of incorrect modelled mixing.

This raises interesting questions about the complexity of the limiting functions associated with the phytoplankton growth (clearly not merely the temperature in this case) and about the capability of the adopted biochemical model not to directly propagate the physical information received and to eventually compensate for the incompleteness of some processes, developing an internal coherence which reduces the sensitivity to many parameters and improves the reaction to different scenarios.

The principal characteristic of station S3 during the investigated period is the presence of the typical tolerant phytoplankton species generally observed in the western Adriatic, namely diatoms and nanoflagellates [46]. Diatoms are well adapted to light-limited environments but generally are more efficient at higher nutrient levels [55]. On the contrary, nanoflagellates have a more favourable affinity for nutrients (especially phosphate [56]), which allows them to survive during the oligotrophic summer periods when light is non-limiting. These features are reasonably reproduced by the generic formulation of the model, but the results of the hindcast do not satisfactorily match the observations.

The major model discrepancies with respect to the observations are found at the surface: the (apparent) reduced duration of the spring bloom, the absence of the smaller summer peaks, and the presence of a winter peak of biomass which is not observed in the data. These seldom capture the fine structures of surface gradients, therefore giving an average measure of, say, the first metre, a bulk measure that is then taken as a model reference. In some cases, this surface layer is well mixed for the physical properties but not for the biological variables.

For instance, the spring bloom in the data extends throughout the months of April and May, apparently lasting until July. Such a feature would require a continuous availability of nutrients, but the analysis of the measured profiles collected in May (figure 8) suggests that this surface peak can hardly be related to local production. Figure 8a shows the profile of
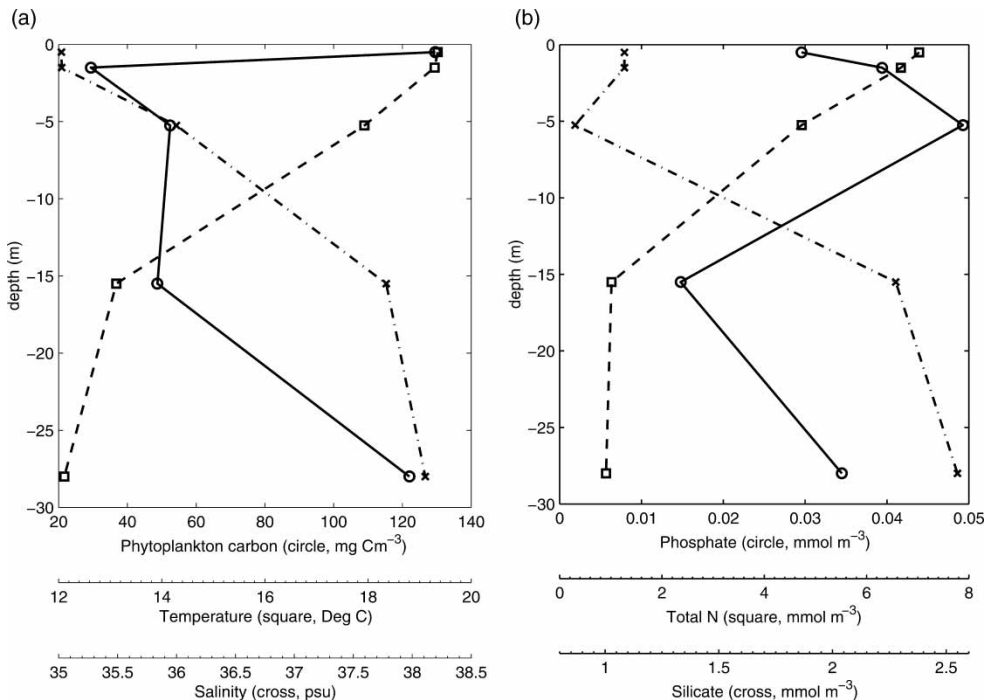

Figure 8. (a) vertical observed profiles of phytoplankton carbon biomass (circle), temperature (square) and salinity (cross) on 10 May 2001; (b) the same for phosphate (circle), total nitrogen (square) and silicate concentrations (cross).

temperature, salinity, and plankton biomass on 10 May 2001. Despite the possibility of slightly inconsistent depths (CTD data are acquired while the probe is descending, biochemical data when the rosette is ascending), phytoplankton seems to show a strong gradient in the first 1.5 m where the physical properties in the very upper layer are instead homogenous.

Among nutrients, only phosphate and, to a limited extent, silicate show an inverse pattern correlation with surface phytoplankton that could be due to local uptake. Nitrogen species are instead apparently unaffected by biology, though they are inversely correlated to salinity, which suggests a riverine source. Therefore, local conditions seem to preclude prolonged bloom. However, conditions may be favourable for a prolonged bloom in areas closer to the Po river mouth where nutrient conditions are in most cases ideal. Indeed, the maximum of phytoplankton in figure 8b is correlated to a noticeable minimum of salinity, which is an indication of advection of fresher water into the region. The strong vertical gradient of biomass can be likely interpreted invoking the lateral advection of a passing biomass. This offers another interesting remark, i.e. that while lateral advection does not make much difference to physical results, it does modify biological results at these timescales. This is a new finding with respect to the work [19], where the same biological model was run with climatological forcing, and the ERSEM model reproduced biological mean conditions observed at the station.

It is also clear that there is a considerable uncertainty related to the use of nutrient and inorganic suspended matter data as BCs (section 4.2). Understanding and quantifying uncertainties in regional modelling are very important nowadays, particularly if models have to be used for environmental policy assessment [14]. The impact of the choice of nutrient BCs and the limited time and spatial resolution of important external forcings such as sediment transports are substantially large, and may hamper the improvements due to the implementation of more sophisticated physical and biological parameterizations. Indeed, as recently shown by Allen *et al.* [57] in the North Sea ROFI, the optics and phytoplankton response in low-light environments are currently poorly resolved, leading to low predictability skills.

6. Conclusions

The present study suggests the following conclusions:

(1) When the physical state of the water column is well simulated with the best available physical model, the choice of the particular second-moment TCMs to embed in the physical model has only a secondary impact on the biology. This suggests that second-moment TCMs have finally 'converged' in recent years.

(2) If we consider only the climatological timescales, lateral advection may be a second-order effect that can be accounted for by time-averaging. Indeed, a climatological ecosystem model behaves quite satisfactorily in stations like S3 [19]. However, when the focus is on predicting the short timescale dynamics, it is more likely that lateral advection cannot be neglected. The current model can produce an accurate physical state but fails to produce the succession of spring–summer blooms observed at S3. This could be due to the absence of lateral advection in the 1-D version of the model used in this study. Future developments are in progress using the 3-D version of ROMS.

(3) The choice of the external BCs has a significant impact on the system evolution. The imposition of low-frequency data on nutrients and optically active particles concentrations can substantially modify the prediction. There is thus an urgent need to collect reliable and high-frequency information on the variability of land-derived inputs of nutrients and suspended sediments to improve the predictive capability of 1-D models. 3-D models are

needed to adequately simulate the advection processes of ROFI regions. However, 3-D coupled physical–biological models have substantial computational requirements, so we suggest that 1-D models are used as intermediate tools for testing new biogeochemical parameterizations and for a basic understanding of the behaviour of lower trophic levels.

Acknowledgements

References

[1] I. Valiela. *Marine Ecological Processes*, 2nd edition, Springer, New York (1995).
[2] K. Wild-Allen, A. Lane, P. Tett. Phytoplankton, sediment and optical observations in Netherlands coastal water in spring. *J. Sea Res.*, **47**, 303–315 (2002).
[3] J. Sharples, C. Moore, T. Rippeth, P. Holligan, D. Hydes, N. Fisher, J. Simpson. Phytoplankton distribution and survival in the thermocline. *Limnol. Oceanogr.*, **46**, 486–496 (2001).
[4] E. Hofmann, C. Lascara. Overview of Interdisciplinary Modeling for Marine Ecosystems. In *The Sea*, Vol. 10, K.H. Brink and A.R. Robinson, pp. 507–540, Wiley, New York (1998).
[5] J. Simpson. Physical processes in the ROFI regime. *J. Mar. Syst.*, **12**, 3–15 (1997).
[6] S. Fonda Umani, C. Sun, E. Feoli, B. Cataletto, M. Cabrini, L. Milani. Is it possible to identify any plankton succession in the Gulf of Trieste (Northern Adriatic Sea)? In *Biology and Ecology of Shallow Coastal Waters*, A. Eleftheriou, A. Ansell, C. Smith, C. (Eds), *28th European Marine Biology Symposium* (1995).
[7] L. Legendre, F. Rassoulzadegan. Plankton and nutrient dynamics in marine waters. *Ophelia*, **41**, 153–172 (1995).
[8] L. Umlauf, H. Burchard. Second-order turbulence closure models for geophysical boundary layers. A review of recent work. *Cont. Shelf Res.*, **25**, 795–827 (2005).
[9] F. Chen, J. Annan. The influence of different turbulence schemes on modelling primary production in a 1D physical–biological model. *J. Mar. Syst.*, **26**, 259–288 (2000).
[10] L. Kantha. A general ecosystem model for applications to primary productivity and carbon cycle studies in the global oceans. *Ocean Modell.*, **6**, 285–335 (2004a).
[11] J.I. Allen, J.R. Siddorn, J.C. Blackford, F.J. Gilbert. Turbulence as a control on the microbial loop in a temperate seasonally stratified Mar. Syst. model. *J. Sea Res.*, **52,** 1–20 (2004).
[12] G. Lacroix, P. Nival. Influence of meteorological variability on primary production dynamics in the Ligurian Sea (NW Mediterranean Sea) with a 1D hydrodynamic/biological model. *J. Mar. Syst.*, **16**, 23–50 (1998).
[13] M. Vichi, P. Ruardij, J.W. Baretta. Link or sink: a model interpretation of the open Baltic biogeochemistry. *Biogeosciences*, **1**, 79–100 (2004).
[14] F. Bernardi-Aubry, F. Acri, M. Bastianini, A. Pugnetti, G. Socal. Phytoplankton contribution to phytoplankton community structure in the Gulf of Venice (NW Adriatic Sea). *Int. Rev. Hydrobiol.*, **91**, 51–70 (2006).
[15] H. Burchard, K. Bolding and M.R. Villarreal. Technical Reports EUR 18745 EN, European Commission (1999).
[16] J. Baretta, W. Ebenhöh, P. Ruardij. The European Regional Seas Ecosystem Model, a complex marine ecosystem model. *J. Sea Res.*, **33**, 233–246 (1995).
[17] J. Baretta-Bekker, J. Baretta, W. Ebenhöh. Microbial dynamics in the marine ecosystem model ERSEM II with decoupled carbon assimilation and nutrient uptake. *J. Sea Res.*, **38**, 195–212 (1997).
[18] J.I. Allen, J.C. Blackford, M.I. Ashworth, R. Proctor, J.T. Holt, J.R. Siddorn. A highly spatially resolved ecosystem model for the north-west European continental shelf. *Sarsia*, **86**, 423–440 (2001).
[19] M. Vichi, P. Oddo, M. Zavatarelli, A. Coluccelli, G. Coppini, M. Celio, S. Fonda Umani, N. Pinardi. Calibration and validation of a one-dimensional complex marine biogeochemical fluxes model in different areas of the northern Adriatic shelf. *Ann. Geophys.*, **21**, 413–436 (2003).
[20] M. Vichi, N. Pinardi, S. Masina. A generalized model of pelagic biogeochemistry for the global ocean ecosystem. Part I: theory. *J. Mar. Syst.*, **64**, 89–109 (2007a).
[21] M. Vichi, S. Masina, A. Navarra. A generalized model of pelagic biogeochemistry for the global ocean ecosystem. Part II: numerical simulations. *J. Mar. Sys.*, **64**, 110–134 (2007b).
[22] L. Kantha. Comments on 'Second-order turbulence closure models for geophysical boundary layers. A review of recent work'. *Cont. Shelf Res.*, **26**, 819–822 (2006).
[23] J.C. Warner, C.R. Sherwood, H.G. Arango, R.P. Signell. Performance of four turbulence closure models implemented using a generic length scale method. *Ocean Modell.*, **8**, 81–113 (2005).

[24] W. Rodi. Examples of calculation methods for flow and mixing in stratified fluids. *J. Geophys. Res.*, **92**, 5305–5328 (1987).

[25] L. Kantha. The length scale equation in turbulence models. *Nonlin. Process. Geophys.*, **7**, 1–12 (2004b).

[26] G. Mellor, T. Yamada. Development of a turbulence closure model for geophysical fluid problems. *Rev. Geophys. Space Phys.*, **20**, 851–875 (1982).

[27] B. Galperin, L. Kantha, S. Hassid, A. Rosati. A quasi-equilibrium turbulent energy model for geophysical flows. *J. Atmos. Sci.*, **45**, 55–62 (1988).

[28] L. Kantha, C. Clayson. An improved mixed layer model for geophysical applications. *J. Geophys. Res.*, **99**, 25235–25266 (1994).

[29] H. Baumert, H. Peters. Second-moment closures and length scales for weakly stratified turbulent shear flows. *J. Geophys. Res.*, **105**, 6453–6468 (2000).

[30] J. Xing, A. Davies. Applications of three dimensional turbulence energy models to the determination of tidal mixing and currents in a shallow sea. *Prog. Oceanogr.*, **35**, 135–205 (1995).

[31] D. Wilcox. Reassessment of the scale-determining equation for advanced turbulence models. *AIAA J.*, **26**, 1299–1310 (1988).

[32] L. Umlauf, H. Burchard, K. Hutter. Extending the k-ω model towards oceanic applications. *Oceanogr. Meteorol.*, **5**, 195–218 (2003).

[33] K. Hanjalic, B. Launder. A Reynolds stress model of turbulence and its application to thin shear flows. *J. Fluid Mech.*, **52**, 609–638 (1972).

[34] D. Wilcox. *Turbulence modeling for CFD*, 2nd edition, DCW Industries, La Cãnada, CA (1998).

[35] L. Umlauf, H. Burchard. A generic length-scale equation for geophysical turbulence. *J. Mar. Res.*, **61**, 235–265 (2003).

[36] L. Kantha, S. Carniel. Comments on 'A generic length-scale equation for geophysical turbulence models' by L. Umlauf, H. Burchard. *J. Mar. Res.*, **61**, 693–702 (2003).

[37] L. Kantha, C. Clayson. On the effect of surface gravity waves on mixing in the oceanic mixed layer. *Ocean Modell.*, **6**, 101–124 (2004).

[38] E. Terray, M. Donelan, Y. Agarwal, W. Drennan, K. Kahma, A.J. Williams III, P. Hwang, S. Kitaigorodskii. Estimates of kinetic energy dissipation under breaking waves. *J. Phys. Oceanogr.*, **26**, 972–987 (1996).

[39] H. Burchard. Simulating the wave-enhanced layer under breaking surface waves with two-equation turbulence models. *J. Phys. Oceanogr.*, **31**, 3133–3145 (2001).

[40] W. Large, J. McWilliams, S. Doney. Oceanic vertical mixing: a review and a model with nonlocal boundary layer parameterisation. *Rev. Geophys.*, **32**, 363–403 (1994).

[41] P. Craig, M. Banner. Modelling wave-enhanced turbulence in the ocean surface layer. *J. Phys. Oceanogr.*, **24**, 2546–2559 (1994).

[42] A. Artegiani, D. Bregant, E. Paschini, N. Pinardi, F. Raicich, A. Russo. The Adriatic Sea general circulation. Part II: Baroclinic circulation structure. *J. Phys. Oceanogr.*, **27**, 97–114 (1997).

[43] M. Zavatarelli, D. Bregant, F. Raicich, A. Russo, A. Artegiani. Climatological biogeochemical characteristic of the Adriatic Sea. *J. Mar. Syst.*, **18**, 227–263 (1998).

[44] A. Bergamasco, M. Gacic. Baroclinic response of the Adriatic Sea to an episode of bora wind. *J. Phys. Oceanogr.*, **26**, 1354–1369 (1996).

[45] I. Cerovecki, Z. Pasaric, M. Kuzmic, J. Brana, M. Orlic. Ten day variability of the summer circulation in the North Adriatic. *Geofizika*, **8**, 67–81 (1991).

[46] A. Pugnetti, F. Acri, M. Bastianini, F. Bernardi Aubry, A. Berton, F. Bianchi, P. Noack, G. Socal. Primary production processes in the north-western Adriatic Sea. In *Proceedings of the AIOL XV Congress*, Vol. 16, Genoa (2003).

[47] R. Reed. On estimating insolation over the ocean. *J. Phys. Oceanogr.*, **17**, 854–871 (1977).

[48] C. Lancelot, J. Staneva, D. van Eeckhout, J.-M. Beckers, E. Stanev. Modelling the Danube-influenced north-western continental shelf of the Black Sea. II: Ecosystem response to changes in nutrient delivery by the Danube river after its damming in 1972. *Estuar. Coast. Shelf Sci.*, **54**, 473–499 (2002).

[49] M. Fasham, H. Ducklow, S. McKelvie. A nitrogen-based model of plankton dynamics in the oceanic mixed layer. *J. Mar. Res.*, **48**, 591–639 (1990).

[50] J.-N. Druon, J. Le Fèvre. Sensitivity of a pelagic ecosystem model to variations of process parameters within a realistic range. *J. Mar. Syst.*, **19**, 1–26 (1999).

[51] J.-Y. Lee, P. Tett, K. Jones, S. Jones, P. Luyten, C. Smith, K. Wild-Allen. The PROWQM physical–biological model with benthic-pelagic coupling applied to the northern North Sea. *J. Sea Res.*, **48**, 287–331 (2002).

[52] M. Vichi, M. Zavatarelli, N. Pinardi. Seasonal modulation of microbial–mediated carbon fluxes in the Northern Adriatic Sea. *Fish. Oceanogr.*, **7**, 182–190 (1998).

[53] P. Ruardij, H.V. Haren, H. Ridderinkhof. The impact of thermal stratification on phytoplankton and nutrient dynamics in shelf seas: a model study. *J. Sea Res.*, **38**, 311–331 (1997).

[54] S. Carniel, M. Sclavo, L. Kantha, C. Clayson. Langmuir cells and mixing in the upper ocean. *Il Nuovo Cimento*, **28C**, 33–54 (2006).

[55] J. Berges, P. Falkowsky. Physiological stress and cell death in marine phytoplankton: Induction of proteases in response to nitrogen or light limitation. *Limnol. Oceanogr.*, **43**, 129–135 (1998).

[56] J. Egge. Are diatoms poor competitors at low phosphate concentrations? *J. Mar. Syst.*, **16**, 191–198 (1998).

[57] J.I. Allen, P.J. Somerfield, F.J. Gilbert. Quantifying uncertainty in high-resolution coupled hydrodynamic-ecosystem models. *J. Mar. Systems*, **64**, 3–14 in press (2007).